ASPS Conference Proceedings 1: 915-923 (2022)

Proceedings of

12th Structural Engineering Convention-An International Event (SEC 2022)

Available at https://asps-journals.com/index.php/acp

Influence of Corrosion Deterioration on Lifetime Seismic Resilience of Highway Bridges

N.R Chirdeep [1], M. Bhargav Chowdary [2], Shivang Shekhar [3, *]

[1] Department of Civil Engineering, Research Scholar, Birla Institute of Technology and Science, Pilani - Hyderabad Campus, Hyderabad 500078, India
[2] Department of Civil Engineering, FD Student, Birla Institute of Technology and Science, Pilani - Hyderabad Campus, Hyderabad 500078, India
[3] Department of Civil Engineering, Assistant Professor, Birla Institute of Technology and Science, Pilani - Hyderabad Campus, Hyderabad 500078, India

Paper ID - 060483

Abstract

Highway bridges across the globe have demonstrated vulnerability to damage during earthquake events. While earthquakes occur infrequently, environmental degradation mechanisms such as chloride-induced corrosion deterioration are continuous and decrease the structural performance over time. There is a need to assess the performance of existing older bridges in India, taking into account the combined threats of corrosion degradation and seismic hazard. In this regard, resilience has emerged as a powerful tool to determine the bridge performance integrating the seismic vulnerability, losses, and recovery functions. This study presents a case-study for lifetime resilience assessment considering the effect of environmental and seismic hazards using a representative two-span semi-integral bridge. Finite element models of the bridge is developed at pristine and four degraded conditions considering chloride-induced corrosion. Nonlinear time-history analyses are conducted on the bridge models to develop time-dependent seismic fragility curves. Further, these fragility curves are used to estimate post-earthquake direct and indirect losses that are combined with suitable recovery models to estimate the functionality and resilience of the bridge. Results obtained from the analysis revealed a degrading trend of the resilience of the bridge as it deteriorates with age, representing the significance of lifetime seismic resilience assessment for estimating the performance of existing aging bridges.

Keywords: Highway bridges, Corrosion deterioration, Seismic fragility, Direct and indirect losses, Lifetime resilience

1. Introduction

Highway bridges structures are essential components of lifeline road transportation systems and play a crucial role in the sustained economic growth of a nation. A majority of highway bridges are built with outdated design specifications and suffer from age-related corrosion deterioration. For instance, out of 14,500 bridges on National Highways in India, more than 1700 are reported to be in distressed conditions requiring repair and rehabilitation, and over 2000 bridges are considered to be old and weak and thereby demanding reconstruction [1]. Corrosion degradation results in the reduction of the load-carrying capacity of the bridges and the failure probability of such bridges is further increased when located in the region of moderate to high seismicity. For instance, the failure of the old Surajbari bridge in India during the 2001 Bhuj earthquake was accelerated due to the distress conditions as a result of reinforcement bars corrosion in the aggressive environment [2]. Bridge damage from such events causes serious disturbance to transportation networks, compromising their functionality, thereby affecting the post-hazard emergency response and socio-economic recovery of widespread regions. Therefore, to ensure the social and economic well-being of the country, there is a need to assess the lifetime performance of existing older highway bridges under joint aging and seismic threats.

In the last few decades, resilience has been widely used as a performance indicator for infrastructural systems such as bridge, and account for vulnerability, losses, and post-disaster recovery measures. [3–8]. In all the above-mentioned studies, to estimate resilience, seismic fragility curves are used to express vulnerability, and the associated losses (direct and indirect) that arise due to post-event bridge repair and loss of bridge functionality are estimated along with consideration of suitable recovery models to represent post-event recovery of damaged bridges. These studies, however, did not consider continuous corrosion deterioration of bridges that may emerge crucial while assessing the lifetime resilience. Recently, for a representative corroded bridge, Biondini et al. [9] estimated the time-dependent resilience using base shear and displacement ductility as functionality indicators. The study, however, did not consider direct and indirect losses owing to bridge seismic damage. Dong and Frangopol [10] assessed the seismic resilience of a highway bridge incorporating time-dependent fragility curves, losses, and simplified linear recovery models. More recently, Vishwanath and Banerjee [11], Huang and Huang [12], and

*Corresponding author. Tel: +914066303-759; E-mail address: shivangshekhar@hyderabad.bits-pilani.ac.in

Published online: December 19, 2022
doi:10.38208/acp.v1.602

Xiaohui et al. [13] estimated the lifetime seismic resilience of bridges utilizing time-dependent fragility curves, direct and indirect losses arising from bridge damage, and recovery functions.

Pertaining to India, the mediocre performance of highway bridges has been exposed numerous times during past earthquake events such as the 1984 Cachar earthquake, the 1997 Jabalpur earthquake, the 1999 Chamoli earthquake, and the 2001 Bhuj earthquake, among others. Past studies by Goswami and Murty [14] and Shekhar et al. [15] indicated the high vulnerability of older bridges in India due to the non-inclusion of ductile detailing principles in the seismic design codes. The studies, however, did not consider the impact of continuous corrosion deterioration that may emerge crucial for bridges located in harsh environmental exposure conditions. Hence, there is a need to evaluate the performance of existing older bridges in India considering combined threats stemming from corrosion deterioration and earthquake hazards. Such explorations will provide an understanding on the lifetime seismic resilience of older bridges designed and detailed as per Indian codal provisions.

Addressing existing drawbacks and augmenting past research, this study estimates the lifetime seismic resilience of a deteriorating highway bridge in India. The next section of the paper elaborates on the framework for estimating seismic resilience that includes vulnerability, losses, and recovery models. Next, a 2-span case-study bridge designed as per Indian standards is introduced, and time-dependent corrosion modeling of bridge pier is elaborated considering chloride-induced corrosion deterioration. This section also presents the finite element modeling of the deteriorated bridge pier capable of capturing different failure modes. The subsequent section discusses the development of time-dependent vulnerability model using nonlinear time-history analysis. Lastly, the study utilizes the developed fragility curves, direct and indirect losses, and recovery function to estimate the lifetime seismic resilience of the bridge. The paper ends with key conclusions and recommendations for future explorations.

2. Framework for Lifetime Seismic Resilience Assessment

In the last few decades, resilience has been widely used as a performance indicator for infrastructure systems such as health care [16], power transmission [17], water supply [18], and transportation systems [4]. In these studies, resilience is defined as a dimensionless quantity that measures the rapidity of the system to recover from a damaged state to the pre-damaged functionality level. The two key components used to assess any system resilience are the loss due to natural events and the system's post-event performance recovery. For a single earthquake event, resilience can be expressed as [16]:

$$R = \int_{t_{oE}}^{t_{oE}+T_{LC}} \frac{Q(t)}{T_{LC}}\, dt \tag{1}$$

where, $Q(t)$ is the time-dependent functionality (and is an integrated measure of structural vulnerability, post-event losses, and recovery processes), and T_{LC} is a controlled time used to evaluate resilience. Fig. 1 depicts the system

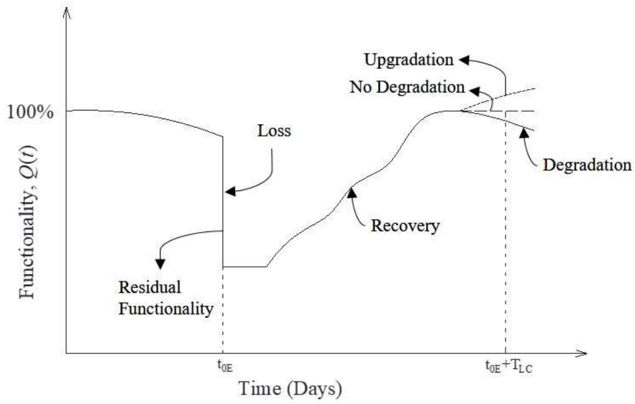

Fig. 1. Schematic representation of seismic resilience of degrading bridges

functionality before and just after a seismic event and during the post-event recovery process. Therefore, seismic resilience can be calculated from the normalized area under the functionality curve between the time of occurrence of the seismic event (t_{0E}) and a time instant, $t_{0E}+T_{LC}$ as shown in Fig. 1. The functionality $Q(t)$ can be defined for a time instant t as follows [16]:

$$\begin{aligned} Q(t) = 1-[L(I,T_{rec})\times\{H(t-t_{oE})-...\\ ...H(t-(t_{oE}+T_{rec}))\}\times f_{rec}(t,t_{oE},T_{rec})] \end{aligned} \tag{2}$$

where, $L(I, T_{rec})$ is the loss function, $H(\cdot)$ is the Heaviside step function, f_{rec} is the recovery function that depends on recovery time (T_{rec}), T_{rec} is the time required to recover the functionality of a damaged bridge for earthquake event, t_{0E} is the time of occurrence of earthquake event. The loss function is calculated utilizing the bridge system vulnerability under earthquake event. As observed from Equation (2), the functionality $Q(t)$ = 1.0 in case of no loss and $0<Q(t)<1.0$ when there is loss due to earthquake damage. As a result, resilience is expressed as a percentage of overall functionality, and R = 100% for a completely usable system with no degradation and loss of functionality after a severe event. Otherwise, depending on the level of damage and loss of system performance due to seismic activity, $0<R<100\%$.

Fig. 2 outlines the overall framework for lifetime seismic resilience assessment of aging highway bridges considering environmental (airborne chloride exposure) and natural (earthquake) hazards. The lifetime resilience framework is illustrated using a five-step approach [Steps (A) to (E)]. Step (A) represents the consideration of location-specific environmental exposure (airborne chloride penetration) and the development of corrosion deterioration path of the bridge at different points in time along the design service life of the bridge. The time-dependent corrosion deterioration model includes cross-sectional area loss of reinforcement and associated secondary effects such as reduction in core and cover concrete strength, and reduction in steel strength and ductility. A detailed discussion on time-dependent corrosion deterioration modeling, including initiation and propagation phases, is given later in Section 3.1. Utilizing the corrosion deterioration model, Step (B) involves the development of statistically identical but nominally different finite element

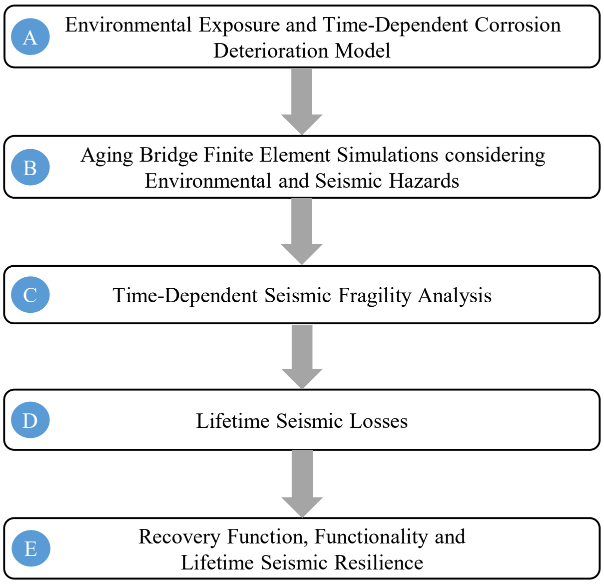

Fig. 2. Seismic resilience framework for aging highway bridge

aging bridge models at different points in time along the service life. These models reflect uncertainty in material characteristics as well as deterioration parameters. Next, each bridge sample is paired with a ground motion record from a suite of accelerograms representative of the case-study region to conduct nonlinear-time-history analyses. Section 3.2 provides a detailed discussion on finite element modeling and simulations of the case-study bridge considering corrosion deterioration.

Step (C) involves the development of time-dependent seismic fragility curves of the bridge using a two-step approach. First, the results from Step (B) are utilized to develop probabilistic seismic demand models (PSDMs) of the bridge at different points in time along the service life. The second step involves the development of seismic fragility curves using the demand model and limit state capacity model of different damage states (Slight, Moderate, Extensive, and Complete). The time-dependent seismic fragility for a particular damage state *DS* follows lognormal distribution and is estimated as [19]:

$$P[DS(t) \mid PGA] = \Phi\left(\frac{\ln(PGA) - \ln(med(t))}{\zeta(t)}\right) \tag{3}$$

where, $P[DS(t)|PGA]$ is the probability of damage state exceedance at time t given a *PGA* (peak ground acceleration) intensity, $med(t)$ is the median of lognormal distribution for fragility function at time t, and $\zeta(t)$ is the dispersion of fragility function at time t.

In Step (D), loss functions are derived considering direct and indirect losses occurring due to bridge damage during an earthquake event. The direct loss (L_D) defines the financial value related to the post-disaster repair and rehabilitation of damaged bridge components and is calculated by multiplying failure probability obtained from fragility curves (Equation (3)) with damage ratios. The damage ratio is considered as 0.03, 0.08, 0.25, and 0.67, respectively for slight, moderate, extensive, and complete damage states of bridge [7,20,21]. Indirect losses (L_I) occur due to the interrupted bridge functionality after the seismic event E, and include operating cost of vehicles on detour (C_{op}) [5] and cost due to vehicle time loss (C_{TL}) as a consequence of bridge damage [22]. This cost is further divided by bridge replacement cost to obtain the normalized indirect loss (L_I). Lastly, the loss function $L(I, T_{rec})$ can be computed by adding direct loss (L_D) and indirect loss (L_I).

Step (E) of the framework helps to calculate the lifetime resilience of the case-study bridge using vulnerability information obtained from fragility curves, direct and indirect losses owing to seismic damage, and suitable recovery models. Based on the available resources to respond to the earthquake damage, Cimellaro et al. [16] suggested different recovery functions such as linear, exponential, and trigonometric. Deco et al. [4] suggested recovery functions based on the bridge damage state, type and location of damage, and restoring techniques. The recovery path can also be represented using sigmoidal curve [23], and is utilized in this study. The post-event recovery time (T_{rec} in Equation (2)) for different damage is adopted from HAZUS [20].

Until now, this paper has elaborated on the framework for seismic resilience assessment, the next section introduces the representative case-study aging highway bridge with discussions on the finite element modeling and chloride-induced corrosion deterioration of bridge pier.

3. Representative Case-Study Bridge: Deterioration Mechanisms and Finite Element Modeling

The influence of corrosion deterioration on the lifetime seismic resilience assessment is presented using a representative two span semi-integral bridge adopted from the work of Shekhar et al. [15]. In a semi-integral bridge, the deck is continuous over the intermediate piers but has bearings at the abutments. Fig. 3 shows the general layout of the case-study bridge consisting of two 20 m spans, a 7.5 m wide two-lane bridge deck, along with cross-section details of the bridge pier. The design concrete strength of the substructure and superstructure is assumed to be 35 MPa and 40 MPa, respectively. This superstructure configuration results in a gravity load of 3500 kN on the reinforced concrete bridge pier. The diameter (D) and height of the pier (H) are adopted as 1.4 m and 6.72 m, respectively. The bridge is assumed to belong to older non-seismic design era, therefore, the pier is designed for gravity loads alone. For this design era, piers were typically designed for negligible lateral forces, and minimum reinforcement criteria governed the design and detailing [15,24]. The longitudinal and transverse reinforcement details of the pier are mentioned in Fig. 3. The following subsections first describe the time-dependent deterioration modeling of the bridge piers due to corrosion, followed by the finite element (FE) modeling approach.

3.1. Time-Dependent Deterioration Modeling of Case-Study Bridge Pier

Reinforced concrete bridges exposed to severe environmental conditions may often experience chemical deterioration that could manifest in different forms. Among these various deterioration mechanisms, chloride-induced corrosion deterioration has emerged as a matter of increasing concern [25,26] and hence considered in this study. Multiple bridge components experience continuous corrosion deterioration during their design life, and among them, the corrosion deterioration of bridge piers significantly impact the seismic response [27]. The subsequent paragraph develops the time-dependent deterioration model of the bridge for airborne chloride exposure condition (Step A of Fig. 2).

Corrosion deterioration in bridge piers, as in other reinforced concrete structures, initiates after a time-gap referred to as corrosion initiation time (T_i). During this period, chloride ions progressively ingress into the concrete cover and depassivates the reinforcing steel initiating corrosion. Chloride ion permeability is modelled according to Fick's second law of diffusion. The corrosion initiation time in years (T_i) can be calculated using an approximate solution to Fick's law, as per IRC 2002 [28].

$$T_i = \frac{C_0 c^2}{12 D_C \left(\sqrt{C_0} - \sqrt{C_{th}}\right)^2} \tag{4}$$

where, C_0 is the equilibrium chloride concentration (kg/m^3) on the exposed surface of concrete, c is the concrete cover thickness (mm), D_C is the coefficient of chloride diffusion through concrete (mm^2/year), and C_{th} is the threshold value of chloride concentration (kg/m^3). However, there are uncertainties in all of these variables, which affects the initiation time. To estimate the corrosion initiation time, this study assumes airborne chloride exposure condition and associated probabilistic distribution of the parameters are adopted from past literature [29–31] and reported in Table- 1. For the case-study bridge structure, based on the probabilistic analysis considering the uncertainty of the above-mentioned parameters, the mean corrosion initiation time is estimated as 20 years (Fig. 4).

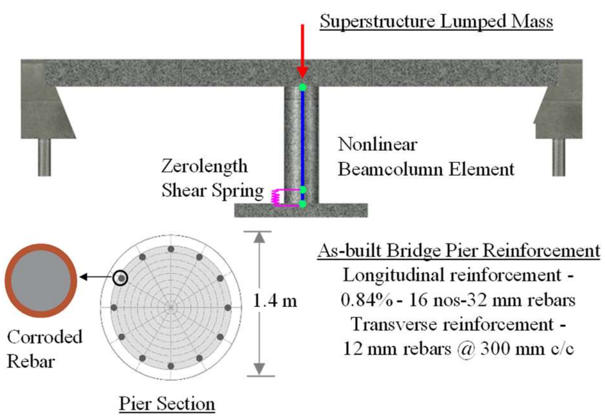

Fig. 3. General layout of case-study bridge showing details of as-built bridge piers and FE modeling. Modeling of piers depends on the point in time along service life.

Table- 1. Probability distribution of the parameters involved to estimate corrosion initiation time and rate of corrosion considering airborne chloride exposure condition

C_0: Equilibrium chloride concentration (kg/m^3) (Vu and Stewart 2000)		
Distribution: *Lognormal* (λ, ζ)	λ	ζ
	0.9696	0.4738
c: Concrete cover depth (mm)		
Distribution: *Normal* (μ, σ)	μ	σ
	40	8
D_C: Chloride diffusion coefficient (mm^2/year) (Vu and Stewart 2000)		
Distribution: *Lognormal* (λ, ζ)	λ	ζ
	3.9218	0.6678
C_{th}: Threshold chloride concentration (kg/m^3) (Vu and Stewart 2000)		
Distribution: *Uniform* (a, b)	a	b
	0.60	1.20
r_{corr}: Rate of corrosion (mm/year) (Firodiya et al. 2015)		
Distribution: *Lognormal* (λ, ζ)	λ	ζ
	-2.22	0.20
N (μ, σ) refers to Normal distribution with parameters μ and σ representing mean and standard deviation; LN (λ, ξ) refers to Lognormal distribution with parameters λ and ξ, which are the mean and standard deviation of the corresponding Normal distribution; U (a, b) refers to Uniform distribution with parameters a and b representing lower and upper bound.		

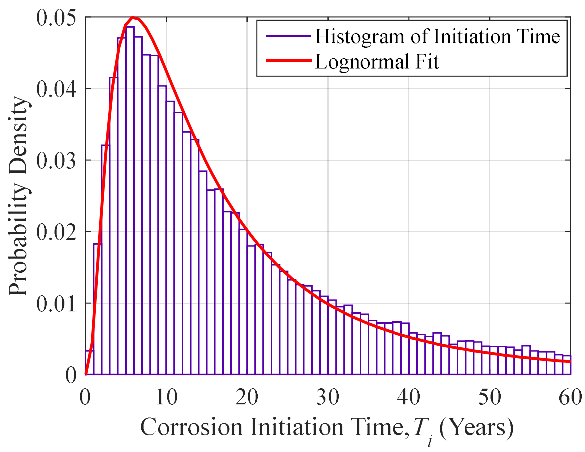

Fig. 4. Probability density function of corrosion initiation time

Following the initiation phase, the corrosion rate during the propagation phase is critical to determine the extent of deterioration primarily in the form of reinforcing steel area loss along with other secondary effects such as concrete and steel strength reduction. The corrosion propagation phase is characterized by the formation of small independent pits or cracks along the steel bar that with time lead to wider cracks resulting in uniform corrosion [32]. At time t_p after the corrosion initiation, the uniform cross-sectional area reduction of reinforcing steel [$A_{st}(t)$] can be estimated as:

$$A_{st}(t) = \frac{n\pi}{4}[D_i - (r_{corr} \times t_p)]^2 \tag{5}$$

In the above equation, n is the number of reinforcing bars, D_i is the initial nominal diameter of a bar, t_p is the elapsed time in years after initiation of corrosion, and r_{corr} is the corrosion rate for the bars in mm/year. Firodiya et al. [31] have evaluated corrosion rates for two types of bars (CTD and MS bars) that are typically used in older existing bridges in India using accelerated corrosion tests under wet and dry conditions. The average corrosion rate for CTD bars exposed to dry condition was found to be 0.111 mm/year. Table- 1 shows the lognormal parameters of corrosion rate for CTD bars. Fig. 5 below shows the variation of mean reinforcing steel area with time along with the lower and upper limits of the uncertainty band representing 5th and 95th percentile confidence bounds after incorporating the uncertainties in the corrosion degradation process, as mentioned in Table- 1. As the figure reveals, a 34% decrease in the mean reinforcing steel area is observed after 75 years of exposure, signifying the necessity of considering corrosion deterioration in the lifetime seismic vulnerability assessment of highway bridges. Along with the loss of reinforcing steel area, corrosion deterioration may also lead to several secondary effects, including the reduction of cover and core concrete strength, and reduction in steel strength and ductility.

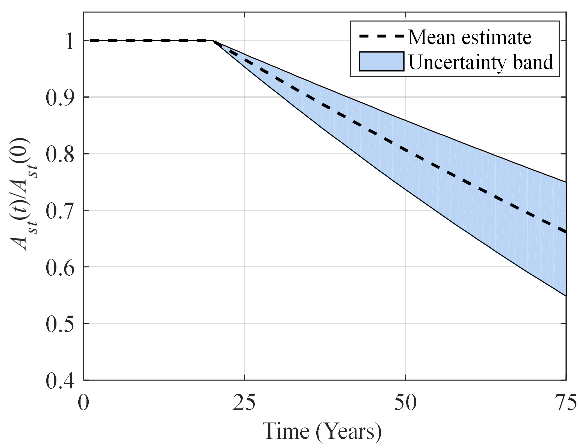

Fig. 5. Variation of mean reinforcing steel area with time along with the lower and upper limits of the uncertainty band representing 5th and 95th percentile confidence bounds.

Corrosion deterioration results in the development of splitting stresses due to the expansive rust products leading to formation of micro-cracks in the cover concrete. These cracks may further widen, resulting in the spalling of the cover. The formulation for deterioration of cover concrete strength is adopted from Biondini & Vergani [33]**.** In addition to strength loss of cover concrete, corrosion deterioration also leads to a reduction of core concrete strength due to area loss of transverse ties. The confined core concrete model proposed by Mander et al. [34] is utilized to estimate the time-dependent core concrete strength.

Additionally, corrosion deterioration along the rebar length results in a reduction of yield or ultimate strength and ductility of steel reinforcement. Experimental investigations on bare or reinforced steel bars revealed that the steel strength reduces linearly with mass loss [35]. This study adopts the time-dependent model proposed by Du et al. [35] that has been widely accepted by other researchers in fragility analysis of corroding structures [26,36]**.** The steel ultimate strain reduction, however, does not follow a linear model as the past experiments reported that the strain reduction values scattered over a large range [27]**.** Therefore, this study adopts the experimental observation of Apostolopoulos and Papadakis [37] in which ultimate strain is observed to be nonlinearly correlated with percentage mass loss and formulation is adopted from Biondini & Vergani [33].

Note that this study assumes the reinforcement steel area loss due to corrosion to be uniform along the length of the column [25,26]. The non-uniform pitting corrosion of steel reinforcement in chloride environment is excluded in the present study for simplicity. However, based on the recommendations from Dizaj et al. [36], while modeling uniform corrosion, other effects of non-uniform pitting corrosion, such as the reduction in steel strength and ductility, are explicitly considered in this study. The next section of the paper elaborates on the analytical modeling of the case-study bridge structure.

3.2. Analytical Modeling of Aging Bridge Piers

The seismic resistance of semi-integral bridges wherein the RC piers are monolithically connected to the deck, is primarily governed by the response of the piers (Kolias et al. 2012), the analytical model of the bridge in this study is idealized as 2D beam-column element representing the bridge pier (Fig. 3). The bridge pier is modeled with a nonlinear beam-column element using the fiber section approach with distributed plasticity, consisting of circular concrete patches and circular layers of reinforcement. The concrete, both confined and unconfined, is modeled using the *Concrete04* material. The longitudinal steel reinforcement is modeled using the *uniaxialmaterial Hysteretic* material within OpenSees. It is noted that the fiber based modeling of RC section can only consider the interaction between biaxial bending and axial force, but not the effect of shear deformation that can be crucial in the case of non-ductile pier. A preliminary check on non-seismic designed bridge pier using the ATC-6 [38] methodology reveals that the failure mode of the designed bridge pier with aspect ratio of 3.0 as predominantly flexure-shear. Consequently, based on the recent work of Shekhar et al. [15], the shear behavior is explicitly incorporated by placing a zero-length shear spring (element *zeroLength* in OpenSees with *uniaxialMaterial LimitState* material) in series with the pier flexure element as shown in Fig. 3. The pier model can now monitor element responses for the user-defined limiting force and deformation and initiate degradation when either the strength or deformation limit curve is reached [15]. The boundary condition for the pier is modeled to be fully restrained as it is assumed that the pier rests on firm soil.

The area loss of steel due to corrosion is modeled as a uniform reduction in rebar diameter along the circumference that includes the time-dependent uncertainty stemming from the corrosion rate. The various secondary effects of corrosion deterioration as mentioned earlier are also incorporated within the finite element modeling of the deteriorated bridge pier. The loss of strength and ductility of rebars is captured by updating the parameters of the *uniaxialMaterial Hysteretic* material. The time-dependent core concrete strength due to corrosion of transverse reinforcement is incorporated by updating the parameters of *Concrete04* material model used to define the column core. The loss of cover strength due to the formation of expansive rust products is modeled by calculating the time-dependent strength of cover concrete and then updating the parameters of *Concrete04* material used to define column cover concrete. The subsequent section utilize the analytical model for time-dependent seismic fragility analysis.

4. Time-Dependent Seismic Fragility Analysis

For seismic fragility analysis, this study considers sources of uncertainty stemming from earthquake ground motion, material and structural modeling parameters, and deterioration parameters. The ground motion characterized by time-histories introduces significant uncertainty in seismic fragility assessment of bridges. These uncertainties can be reduced by considering sufficient number of recorded time-histories representative of the region seismicity. A ground motion suite is adopted from the past work of Shekhar [39]. The 90 selected ground motions have a wide representation of magnitude, and source to site distance and *PGA* range from 0.04g to 0.79g.

In addition to ground motion uncertainties, there exist a number of material modeling and deterioration parameters that may affect the vulnerability of aging bridges. These parameters include material strength such as the strength of concrete and yield strength of steel, and deterioration parameters such as rebar area loss, among others. The chosen mean value of these parameters are specific to the case-study bridge, and additional variation is considered based on the past literature for generating probabilistic finite element models of the bridge.

A full probabilistic analysis is carried out to determine the seismic fragility of case-study bridge (Step B of Fig. 2). Based on modeling and deterioration parameters uncertainty, at different point in time along the service life of the bridge, statistically different yet nominally identical bridge models are developed by sampling across the range of parameters using Latin Hypercube Sampling. 90 analytical bridge models are generated consistent with the number of ground motions in the suite and are then paired randomly with a ground motion time-histories. For each pair, nonlinear time-history analysis is performed and peak demands or engineering demand parameters (*EDP*s) are recorded for bridge pier to derive a relationship between *EDP* and the ground motion intensity. The considered *EDP* for the bridge pier is displacement ductility (μ_Δ). Following NLTHA, PSDMs are developed for each bridge component to estimate median seismic demand using the relation given by Cornell et al. [40].

Subsequent to the development of PSDMs, fragilities are evaluated at different points in time along the service life of the bridge to assess the effect of corrosion deterioration on seismic fragility [Step C of Fig. 2 and Equation (3)]. The limit state capacity for different damage states - slight, moderate, extensive, and complete in terms of displacement ductility are obtained using pushover analysis of bridge pier at different points in time along the service life of the bridge. Note the physical descriptions for different damage states are identified based on the previous studies and are based on strain criteria of steel and concrete, and shear failure of the pier [15].

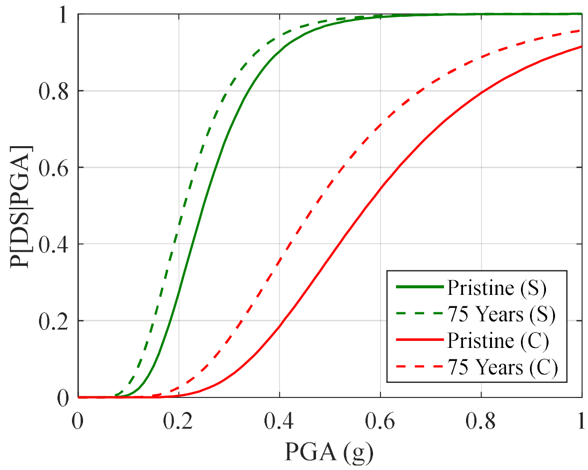

Fig. 6. Comparison of seismic fragility curves of bridge for Slight (S), and Complete (C) damage states under pristine and deteriorated state (75 Years)

Fig. 6 depicts the seismic fragility curves for the case-study bridge in pristine and aging (75 years) condition for the slight and complete damage states. As the figure illustrates, compared to pristine bridge conditions, there is increase in fragilities of the bridge at 75 years of service life when exposed to airborne chloride environmental exposure. The corrosion of bridge pier results in a reduction of strength and stiffness of the bridge pier leading to increase in vulnerability. Although not shown here, similar trend of increased vulnerability i.e. decrease in median fragility [$med_m(t)$] (*PGA* corresponding 50 % failure probability) is observed for other damage states. It is also noted that slight increase in dispersion [$\zeta_m(t)$] is also observed over time indicating increased uncertainty in predicting median *PGA* for deteriorated bridge state.

5. Lifetime Seismic Losses and Resilience Assessment

Utilizing the fragility curves developed in the preceding section, first the lifetime losses of the bridge are calculated using Step (D) of the framework (Fig. 2). The direct losses are estimated utilizing the probabilities of exceedance at four damage states obtained from the fragility curves multiplied by the damage ratio of the four damage states taken as 0.03, 0.08, 0.25, and 0.67, respectively. The bridge replacement cost is estimated based on unit area replacement cost multiplied by the deck area. For calculating indirect loss, expected values of traffic-related parameters are assumed from past studies. While some of these repair cost ratios and indirect loss estimates may be different, the present values are adopted due to a lack of available literature within the country. Direct and indirect losses are combined to generate the loss ratio of the bridge. Fig. 7 shows the variation of loss ratio of the bridge for a wide range of *PGA* and various degraded conditions of the bridge. As observed from the result, the loss ratio increases with an increase in *PGA* and degradation of the bridge.

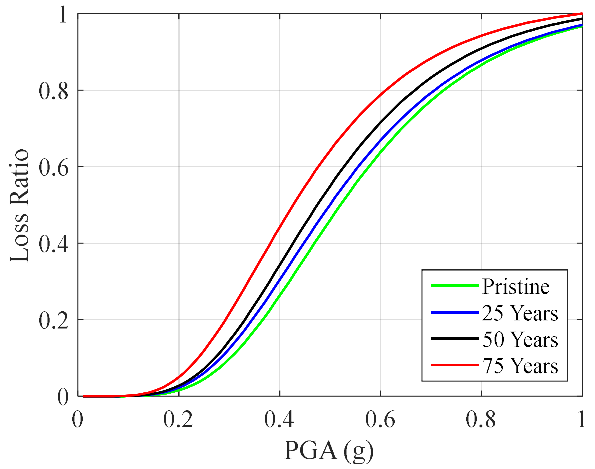

Fig. 7. Variation of loss ratio with PGA for various degraded conditions of the bridge

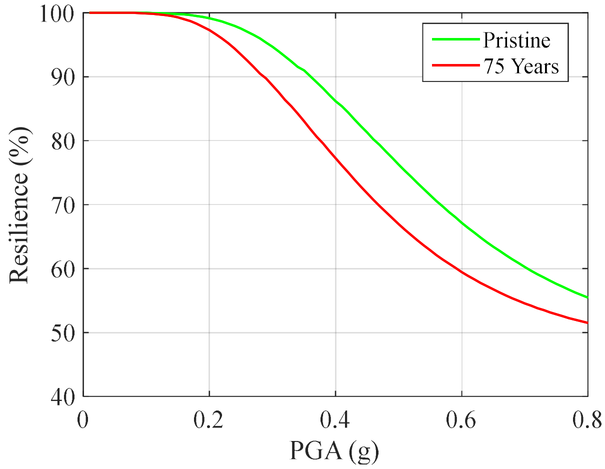

Fig. 8. Resilience of the pristine and 75-year old bridge for various earthquake hazards represented using PGA

Next, following Step (E) of the framework, damage-specific recovery functions (f_{rec}) and control time are used to compute functionality and resilience of the bridge for different levels of earthquake hazards (PGA = 0.1g to 1.0 g) and degrading conditions (bridge age = 0, 25, 50, and 75 years). The probable damage states of the bridge under different degraded conditions for various earthquake intensities are obtained from the time-dependent seismic fragility curves applying the approach mentioned in Karamlou and Bocchini [41]. The functionality and resilience are computed using Equations (2) and (1), respectively.

Fig. 8 shows the resilience of the bridge as a function of earthquake hazard (PGA) for pristine and 75-year degraded conditions. It is observed that resilience decrease with an increase in PGA, and the resilience of 75-year old bridge is lesser than the pristine bridge. The resilience decreases to 56% and 47%, respectively, for the pristine and 75-year degraded bridge as PGA increases from 0.1g to 0.8g. Fig. 9 shows the lifetime resilience of the bridge for PGA = 0.36g and 0.72g. As observed, the resilience decreases across the life-cycle as the bridge continues to degrade over 75 years. The higher the PGA more is the decrease in resilience.

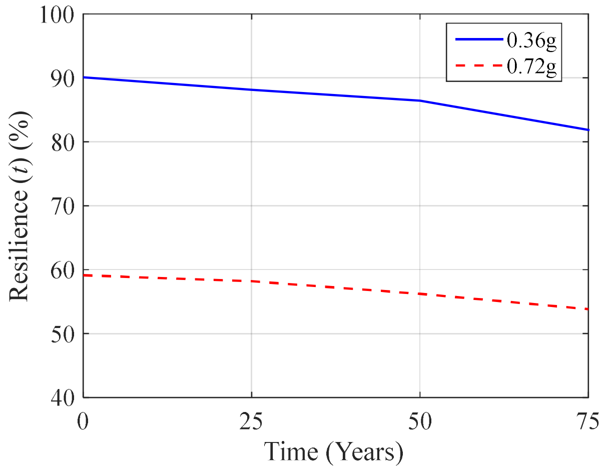

Fig. 9. Lifetime resilience of the bridge for PGA = 0.36g and 0.72g

6. Conclusion

This study presents the impact of chloride-induced corrosion on the lifetime seismic resilience of highway bridge in India. At the onset, the paper presents a five-step framework for lifetime resilience assessment under joint aging and seismic threats. A representative case-study semi-integral bridge is considered, and the lifetime corrosion deterioration path of RC bridge pier under airborne chloride exposure is developed that highlights a significant reduction in embedded rebar cross-sectional area along with other secondary effects such as reduction in mechanical properties of concrete and steel. A full probabilistic analysis considering various sources of uncertainty is conducted to estimate the change in seismic fragility of the deteriorated bridge. A significant increase in vulnerability is observed for cases-study bridge pier. For instance, after 75 years of service life, the median PGA for the complete damage state decreases by 19%.

Next, the lifetime resilience of the case-study bridge is estimated using vulnerability information obtained from fragility curves, direct and indirect losses owing to seismic damage, and recovery models. As observed from the result, the loss ratio increases with an increase in PGA and degradation of the bridge. The resilience decreases to 56% and 47%, respectively, for the pristine and 75-year degraded bridges as PGA increases from 0.1g to 0.8g. Future work will consider the effect of aging and deterioration on the lifetime seismic vulnerability and resilience of older multi-span simply supported bridges in India having several vulnerable components, including abutments, bearings, and piers.

Disclosures

Free Access to this article is sponsored by SARL ALPHA CRISTO INDUSTRIAL.

References

1. Wakchaure SS, Jha KN. Modeling of post-construction failure factors of bridges. Journal of Advances in Management Research, 2011; 8(2): 246–262.

2. Madabhushi SPG, Haigh SK. The Bhuj , India Earthquake of 26th January 2001; A FIELD REPORT BY EEFIT. Society, 2005; 44(January 2001): 207–235.

3. Bocchini P, Frangopol DM, Ummenhofer T, Zinke T. Resilience and Sustainability of Civil Infrastructure: Toward a Unified Approach. Journal of Infrastructure Systems, 2014; 20(2): 04014004.

4. Deco A, Bocchini P, Frangopol DM. A probabilistic approach for the prediction of seismic resilience of bridges. Earthquake Engineering and Structural Dynamics, 2013; 42: 1469–1487.

5. Dong Y, Frangopol DM. Risk and resilience assessment of bridges under mainshock and aftershocks incorporating uncertainties. Engineering Structures, 2015; 83: 198–208.

6. Karamlou A, Bochini P. Computation of bridge seismic fragility by large-scale simulation for probabilistic resilience analysis. Earthquake Engineering and Structural Dynamics, 2015(44): 1959–1978.

7. Venkittaraman A, Banerjee S. Enhancing resilience of highway bridges through seismic retrofit. Earthquake Engineering and Structural Dynamics, 2014(43): 1173–1191.

8. Zheng Y, Dong Y, Li Y. Resilience and life-cycle performance of smart bridges with shape memory alloy (SMA)-cable-based bearings. Construction and Building Materials, 2018; 158: 389–400.

9. Biondini F, Camnasio E, Titi A. Seismic resilience of concrete structures under corrosion. Earthquake Engineering and Structural Dynamics, 2015; 44: 2445–2466.

10. Dong Y, Frangopol DM. Probabilistic Time-Dependent Multihazard Life-Cycle Assessment and Resilience of Bridges Considering Climate Change. Journal of Performance of Constructed Facilities, 2016; 30(5): 04016034.

11. Vishwanath BS, Banerjee S. Life-Cycle Resilience of Aging Bridges under Earthquakes. Journal of Bridge Engineering, 2019.

12. Huang C, Huang S. Seismic resilience assessment of aging bridges with different failure modes. Structures, 2021; 33(March): 3682–3690.

13. Xiaohui Y, Kuangyu D, Yushi L, Bing L. Seismic resilience assessment of corroded reinforced concrete structures designed to the Chinese codes. Earthquake Engineering and Engineering Vibration, 2021; 20(2): 303–316.

14. Goswami R, Murty CVR. Seismic vulnerability of RC bridge piers designed as per current IRC codes including interim IRC : 6-2002 provisions. Journal of The Indian Roads Congress, 2005; 66(2): 379–426.

15. Shekhar S, Ghosh J, Ghosh S. Impact of Design Code Evolution on Failure Mechanism and Seismic Fragility of Highway Bridge Piers. Journal of Bridge Engineering, 2020; 25(2): 04019140.

16. Cimellaro GP, Reinhorn AM, Bruneau M. Framework for analytical quantification of disaster resilience. Engineering Structures, 2010; 32(11): 3639–3649.

17. Shinozuka M, Chang SE. Evaluating the Disaster Resilience of Power Networks and Grids. In Modeling Spatial and Economic Impacts of Disasters, 2004: 289–310.

18. Didier M, Esposito S, Broccardo M, Stojadinovic B. Seismic Resilience of a Water Distribution Network. European Conference on Earthquake Engineering, *(16ECEE)*, 2018.

19. Nielson BG, DesRoches R. Analytical seismic fragility curves for typical bridges in the central and southeastern United States. Earthquake Spectra, 2007; 23(3): 615–633.

20. Federal Emergency Management Agency (FEMA). HAZUS-MH MR4 Multi-Hazar d Loss Estimation Methodology – Earthquake Model: Technical Manual. Department of Homeland Security. Federal Emergency Management Agency*, Washington, ...* 2003.

21. Padgett JE, Dennemann K, Ghosh J. Risk-based seismic life-cycle cost-benefit (LCC-B) analysis for bridge retrofit assessment. Structural Safety, 2010; 32(3): 165–173.

22. Stein BSM, Young GK, Trent RE, Pearson DR. Prioritizing scour vulnerable bridges using risk. Journal of Infrastructure Systems, 1999; 5(September): 95–101.

23. Jónás T. Sigmoid functions in reliability based management. Periodica Polytechnica Social and Management Sciences, 2007; 15(2): 67–72.

24. IRC-6. Standard specifications and code of practice for Road Bridges. 2000.

25. Choe DE, Gardoni P, Rosowsky D, Haukaas T. Probabilistic capacity models and seismic fragility estimates for RC columns subject to corrosion. Reliability Engineering and System Safety, 2008; 93(3): 383–393.

26. Alipour A, Shafei B, Shinozuka M. Performance evaluation of deteriorating highway bridges located in high seismic areas. Journal of Bridge Engineering, 2011; 16(5): 597–611.

27. Andisheh K, Scott A, Palermo A. Seismic Behavior of Corroded RC Bridges: Review and Research Gaps. International Journal of Corrosion, 2016; 2016(3).

28. IRC:SP-60 I. An approach document for assessment of remaining life of concrete bridges. IRC; 2002.

29. Weyers RE. Sevice life model for concrete structures in chloride laden environments. Materials Journal, 1998; 95(4): 445–453.

30. Vu KAT, Stewart MG. Structural reliability of concrete bridges including improved chloride-induced corrosion models. Structural Safety, 2000; 22(4): 313–333.

31. Firodiya PK, Sengupta AK, Pillai RG. Evaluation of Corrosion Rates of Reinforcing Bars for Probabilistic Assessment of Existing Road Bridge Girders. Journal of Performance of Constructed Facilities, 2015; 29(3): 04014067.

32. Broomfield J. Corrosion of steel in concrete: understanding, investigation and repair. 2006.

33. Biondini F, Vergani M. Deteriorating beam finite element for nonlinear analysis of concrete structures under corrosion. Structure and Infrastructure Engineering, 2015; 11(4): 519–532.

34. Mander JB, Priestley M, Park R. Theoretical stress-strain model for confined concrete. Journal of Structural Engineering, 1988; 114(8): 1804–1826.

35. Du YG, Clark LA, Chan AHC. Residual capacity of corroded reinforcing bars. Magazine of Concrete Research,

2005; 57(3): 135–147.

36. Dizaj EA, Madandoust R, Kashani MM. Probabilistic seismic vulnerability analysis of corroded reinforced concrete frames including spatial variability of pitting corrosion. Soil Dynamics and Earthquake Engineering, 2018; 114: 97–112.

37. Apostolopoulos CA, Papadakis VG. Consequences of steel corrosion on the ductility properties of reinforcement bar. Construction and Building Materials, 2008; 22(12): 2316–2324.

38. Council AT. Seismic retrofitting guidelines for highway bridges. National Technical Information Service; 1984.

39. Shekhar S. Influence of corrosion deterioration and design philosophy on seismic vulnerability assessment of highway bridges. Indian Institute of Technology Bombay, Mumbai, 2020.

40. Cornell CA, Jalayer F, Hamburger RO, Foutch DA. Probabilistic Basis for 2000 SAC Federal Emergency Management Agency Steel Moment Frame Guidelines. Journal of Structural Engineering, 2002; 128(April 2002): 526–533.

41. Karamlou A, Bocchini P. Sequencing algorithm with multiple-input genetic operators: Application to disaster resilience. Engineering Structures, 2016; 117: 591–602.